Dynamical Ne K Edge and Line Variations in the X-Ray Spectrum of the Ultra-compact Binary 0614

N. S. Schulz,[1] M. P. Nowak,[1] D. Chakrabarty,[1] and C. R. Canizares[1]

ABSTRACT

We observed the ultra-compact binary candidate 4U 0614+091 for a total of 200 ksec with the high-energy transmission gratings onboard the *Chandra* X-ray Observatory. The source is found at various intensity levels with spectral variations present. X-ray luminosities vary between 2.0×10^{36} erg s^{-1} and 3.5×10^{36} erg s^{-1} . Continuum variations are present at all times and spectra can be well fit with a powerlaw component, a high kT blackbody component, and a broad line component near oxygen. The spectra require adjustments to the Ne K edge and in some occasions also to the Mg K edge. The Ne K edge appears variable in terms of optical depths and morphology. The edge reveals average blue- and red-shifted values implying Doppler velocities of the order of 3500 km s^{-1}. The data show that Ne K exhibits excess column densities of up to several 10^{18} cm^{-2}. The variability proves that the excess is intrinsic to the source. The correponding disk velocities also imply an outer disk radius of the order of $< 10^9$ cm consistent with an ultra-compact binary nature. We also detect a prominent soft emission line complex near the O VIIILα position which appears extremely broad and relativistic effects from near the innermost disk have to be included. Gravitationally broadened line fits also provide nearly edge-on angles of inclination between 86 and 89°. The emissions appear consistent with an ionized disk with ionization parameters of the order of 10^4 at radii of a few 10^7 cm. The line wavelengths with respect to O VIII L$_\alpha$ are found variably blue-shifted indicating more complex inner disk dynamics.

Subject headings: stars: individual (0614) — stars: neutron — X-rays: stars — binaries: ultra-compact — accretion: accretion disks — techniques: spectroscopic

---

[1]Center for Space Research, Massachusetts Institute of Technology, Cambridge, MA 02139.

1.   Introduction

The low mass X-ray binary (LMXB) 0614 has been persistently bright since its detection with *Uhuru* (Forman et al. 1978). It has been identified as a type I X-ray burster (Swank et al. 1978) and thus is an accreting neutron star. A recent study of its very bright X-ray bursts lead to a distance estimate of 3.2 kpc (Kuulkers, in't Zand & Lasota 2009) putting the source a bit beyond earlier projections (Brandt et al. 1992). It is now confirmed to be an atoll source (Mendez et al. 1997) based on its spectral properties (Singh & Apparao 1994; van Straaten et al. 2000) and timing pattern (Ford et al. 1997). A peculiar trait of its X-ray spectrum is the presence of a hard X-ray tail reaching energies beyond 100 keV (Ford et al. 1997) which was modeled as thermal Comptonization at high electron temperatures of greater than 220 keV (Piraino et al. 1999; Fiocchi et al. 2008).

The source has recently become a focus of renewed interest for several reasons. A very recent survey observation covering the source from radio, to infrared, optical, UV and X-ray emissions identified optically thick synchrotron emission from a jet with radiative powers well beyond 10^{32} erg s^{-1} (Migliari et al. 2010). The jet was found to be present in the source's hard state (van Straaten et al. 2000) comparable to what is now found in stellar mass black bole accretors and active galactic nuclei.

This is even more interesting as many indications place 0614 into a rare class of ultra-compact binaries with orbital periods P $\lesssim$ 80 min considered to be near the minimum period for LMXBs with hydrogen-rich main-sequence donors. Shahbaz et al. (2008) favor a 51.3 min binary period which would further classify this system as a neutron star accreting either from a hydrogen-deficient star or a degenerate, likely white dwarf companion (Verbunt & van den Heuvel 1995). Observations with *Chandra* determined Ne K shell absorption significantly above the expectation from ISM column densities (Paerels et al. 2001). This seems to support the suggestion by Juett, Psaltis & Chakrabarty (2001) and Juett & Chakrabarty (2005) that the enhanced Ne/O ratios determined from X-ray spectra point to a low-mass, neon-rich degenerate white dwarf companion in 0614 and other very low period binaries and that these binaries are all ultra-compact. VLT spectroscopy confirms the deficiency of H and He in the accretion disk of the proto-type ultra-compact source 4U 1626-67 and in 0614, again pointing towards an ultra-compact nature (Werner et al. 2006). However, these data show a peculiar lack of Ne line which seems in stark contrast to the X-ray findings and it was suggested that the donor could be an eroded C/O white dwarf with no excessive Ne overabundance.

We observed 0614 with the high resolution transmission grating spectrometer (HETGS) onboard *Chandra* for about 2.5 days in order to study in depth the X-ray absorption properties. In this paper we specifically focus on the intrinsic source properties, i.e. the nature of

its X-ray continuum emission, possible broad line emissions, excess K edge properties, and spectral variability.

2. Chandra Observations

The *Chandra* HETGS observations were performed during Cycle 10 of the mission and are part of our guaranteed time program. The detailed observation dates and parameters are listed in Table 1. The total amount of 200 ksec of observating time was arbitrarily split into four pieces of about 40 to 60 ksec duration, which were taken over a total time span of about 4.5 days.

All observations were processed using CIAO4.2 with the most recent CALDB products using the tools offered by the on-line transmission grating catalog (TGCAT[1]). The zero-order point spread function (psf) was sufficiently piled up; therefore an improved zero-order postion was determined using *findzo.sl* which uses the the intersection of the psf readout-out streak and the HETG dispersion tracks [2]. Figure 1 shows the zero order point determination for the psf in OBSID 10759. Proper positioning is absolutely crucial for this study. For all the observations we generated spectra and analysis products for the 1st orders only.

Pre-screening of the data revealed variability between observation segments and given the brightness of the source we integrated one spectrum for each segment. For the Ne K edge study we also split the observations into consecutive sub-segments in order to investigate spectral changes on smaller time scales. We fitted all spectral orders simultanously, for plotting purposes we co-added and also re-binned all 1st orders. The spectral analysis was performed using the latest version *ISIS*[3] with imported *Xspec.v12* functions for spectral modeling. Uncertainties ar listed as 90% confidence limits calculated using the multi-parameter grid search utility *conf_loop* in *ISIS*.

2.1. Light Curves and Fluxes

Figure 2 shows the light curves of the four observations. The curves, binned to 200 sec bins, appear fairly smooth with mostly gradual intensity changes. The first three observations

---

[1]see http://tgcat.mit.edu/

[2]see also http://asc.harvard.edu/ciao/threads/

[3]see http://space.mit.edu/ASC/ISIS

are at very similar intensity levels. The observations show gradual intensity variations at a 15% to 45% level. Obsid 10857 is brightest with a factor ~ 2 higher average intensity. There are no rapid changes in the light curves and we also do not detect type I burst activity. Three observations show intermittent broad flare-like events lasting for several 1000 sec.

The source fluxes (0.5 – 10 keV) range from $(1.17 \pm 0.02) \times 10^{-9}$ erg cm^{-2} s^{-1} in OB-SID 10858 to $(2.05 \pm 0.02) \times 10^{-9}$ erg cm^{-2} s^{-1} in OBSID 10760. With an interstellar column density of 3.3×10^{21} cm^{-2} (Piraino et al. 1999; Migliari et al. 2010) this translates to source luminosities in the range of $(2.0 - 3.5) \times 10^{36}$ erg s^{-1} at a source distance of 3.2 kpc (Kuulkers, in't Zand & Lasota 2009), which is consistent with a recent analysis of atoll sources by Linares, van der Klis & Wijnands (2008) and correponds to about 0.01 L_{Edd}.

In order to further investigate source state properties we also computed color-color and hardness-intensity diagrams, The *Chandra* HETG bandpass with respect to *RXTE* is limited and we do not have the same energy bands to compute hardness ratios available as is traditionally done with broadband instruments such as *RXTE* , *GINGA* , and *EXOSAT* . As we have done in Schulz et al. (2009), we chose f_{xs}=flux(0.5 keV – 2.5 keV), f_{xm}=flux(2.5 keV – 4.5 keV), and f_{xh}=flux(4.5 – 8.0 keV) and thus for the hard ratio f_{xh}/f_{xm} and the soft ratio f_{xm}/f_{xs}. The diagram in Figure 3 (left) shows that the broadband colors of each observation overlap in a small area. There is no variation in soft ratio, but some variations in the hard ratio are similar to the findings by by Linares, van der Klis & Wijnands (2008) using *RXTE* data. The hardness-intensity relations indicate that that the hard ratio variations are present at all intensities.

2.2. Continuum Spectra

Two spectral continuum models have been suggested previously. One was provided by Piraino et al. (1999) which for our relevant bandpass suggests a powerlaw plus blackbody model. The other one was suggested by Migliari et al. (2010) and consists of a powerlaw plus a blackbody plus a disk blackbody model. Both models also featured a soft gaussian line feature in the oxygen region (see also Schulz 1999).

In all our fits we applied the recently released *Tbnew* function in *Xspec* which is based on recent high resolution studies (Juett, Schulz & Chakrabarty 2004; Juett et al. 2006) and uses ISM abundance from Wilms, Allen & McCray (2000). In order to find an estimate for the interstellar column towards 0614 we at first left the NH parameter free without any adjustment to any elements. The fit at the O K edge provided a column of $(3.31 \pm 0.04) \times 10^{21}$ cm^{-2} which is consistent with the findings by previous studies. We then fixed the NH column

in the ISM to this value during all fits. The powerlaw plus blackbody model alone generally fits to our data <10 Å with some waviness left in the residuals. A hard blackbody as suggested by both approaches was necessary to fit the spectral band <3 Å and we add this component into all our fits with a normalization ($A_{bb} =\sim 1 \times 10^{35}$ erg s^{-1} at 3.2 kpc) and temperature (~ 1.22 keV) very similar to the one suggested by the studies of Piraino et al. (1999) and Migliari et al. (2010).

At higher wavelengths (> 10 Å) the simple powerlaw approach breaks down and we observe significant deviations. Adding a spectral component such as another soft blockbody or a soft disk blackbody did not result in acceptable fits. Figure 4 shows all the relevant features in the soft part of the spectrum, which consist of O, Ne, and Mg K edges at 22.9, 14.28, and 9.48 Å, respectively, an Fe L edge around 17.5 Å and a broad excess around 18 Å. Figure 5 (top panels without obsid labels) shows the residuals of the unmodified continuum fits for each observation sequence. One strong residual appears at the location of the Ne K edge, another one is observed between 16 and 20 Å. Some smaller residuals appeared at Mg K and some waviness around 11 Å and in some observations near 5 Å. In order to avoid adding separate edge components to the broadband analysis we used the abundance parameter in the the *Tbnew* function to fit additional variable edge depths. Our fits show that the emission component is so broad that the soft residuals can only be fit by a single soft Gaussian line component similar to the one found in previous analyses (Piraino et al. 1999; Migliari et al. 2010) and now very recently in *XMM-Newton* RGS data Madej et al. (2010).

The new residuals are plotted in Figure 5 (bottom panels with obsid labels). The adjustments provide an acceptable fit to all spectra with reduced χ^2 values between 1.3 and 1.7 in the worst case. Powerlaw indices were quite similar in all observations but varied between 2.13 and 2.25, whereas normalizations A_{pl} varied between 0.35 and 0.65 ph cm^{-2} s^{-1} Å^{-1}. Table 2 summarizes the continuum components as well as the fits results for the broad line. In all cases the fits to the spectra required significant increases of the Ne K optical depth. In OBSID 10858 the fits also suggested a significant adjustment to the Mg K edge.

3. Ne K Edges Morphology

In Figure 6 we show the edge appearance over the entire exposure. The edge contains red- and blue-shifted components in addition to the ISM contribution. From the fits it also becomes apparent that the Ne optical depth changes with time. There is a sharp residual in the fits (see also Figure 4) at 14.3 Å which indicates some issues with the actual location

of the edge in the spectra. The interstellar Ne edge structure and value has been studied in detail by Juett et al. (2006) and its wavelength has been found to be 14.295±0.003 Å coincident with the Ne I $1s - 3p$ transition consistent with the standard model Gorczyca (2000). The following analysis focusses on the local structure and now applies a local model consisting of ISM absorption, a powerlaw, and the explicit Ne edge function in the range between 13 and 15 Å. We again fixed the interstellar contribution to the edge to a column density of 3.3×10^{21} cm^{-2}. This density corresponds to an optical depth τ_{ISM} of 0.17 (N$_{Ne}$ = 4.57×10^{17} cm^{-2}), which is more than twice the detection threshold at this particular wavelength. For the observed continuum levels an edge with an optical depth of about 0.04 can be detected. Note, that in terms of significance this only corresponds to about 1σ above the continuum. However, in contrast to line detections which require much higher significances at the centroid wavelength, the edge detection threshold is an integral quantity over several bins above and below the edge (see Schulz et al. 2002).

We noticed that the morphology of the edge changes on timescales smaller than our observation segments and we split these segments into several equally timed and consecutive intervals. The exposure of these sub-segments was chosen to provide enough counts in each spectrum for good statistics during spectral fitting. In conjunction with the good time intervals this lead to 18 sub-segments with 9.7 ksec, one with 8.6 ksec, and one with 5.5 ksec. We also approximate the edge smearing effect in a very simple way by adding a blue and a red-shifted component to the Ne edge fits of the sub-segments. The optical depths $\tau_{source} = \tau_{bNe} + \tau_{rNe}$ are in excess of the one produced by the interstellar columns, i.e. τ_{Ne} = $\tau_{source} + \tau_{ISM}$. The fit values vary from sub-segment to sub-segment indicating the more continuous change with time. This explains the different appearance of the edge in all the segments and sub-segments. Blue-shifted depths τ_{bNe} vary from 0.057 to 0.274, red-shifted depths τ_{rNe} from 0.013 to 0.245. The total source depth τ_{source} (in excess of τ_{ISM}) then varies from 0.131±0.034 to 0.444±0.130 which corresponds to a Ne column density range of 3.6×10^{17} cm^{-2} to 1.2×10^{18} cm^{-2}.

Figure 7 shows two examples of edge smear, one with a low spread of about 0.15 Å (top), and one with a high spread of about 0.65 Å. The measured shifts imply velocity smears ranging from about 2000 to 15000 km s^{-1} as plotted in Figure 8. The measured blue-shifts show variations in all observation segments. Figure 8 plots the total velocity smear which is comprised of added shifts of the edge on the red and blue side versus the similarly added optical depths (τ_{source}). Note that observed smears are generally higher than the one expected from an orbital binary period of 51.3 min (Shahbaz et al. 2008). The uncertainties specifically for high values are fairly large and most segment values agree with values between 7000 and 8000 km s^{-1}, which after subtracting a possible binary orbital contribution translates to dynamic velocities between 3100 km s^{-1} and 3700 km s^{-1}.

The resulting optical depth and smear velocities do not seem to reveal any specific pattern with time. Nevertheless, we tested if we could find recurring patterns by folding the light curve by several periods in the system as suggested by Shahbaz et al. (2008). We used OBSID 10759 for such a test and generated and fitted six phase-binned spectra. We applied periods of 41 min, 51 min, 62 min, and 120 min. In no cases did we observe evolving patterns, which leads us to conclude that the observed variations are random with respect to possible short orbital periods. We do not have enough statistics to fully investigate the time scale of change in the edge morphology other than observe that it is likely of the order of $<< 10^4$ sec.

3.1. Broad Line Emission

Previous studies always required to include a strong broad emission line feature near the oxygen region into any spectral fit of 0614 (Singh & Apparao 1994; Piraino et al. 1999; Schulz 1999; Migliari et al. 2010). The HETG spectra also require such a feature between 17 and 19 Å as is shown in the residuals in Figure 4 and 5. The feature is broad and is fully resolved in all fits. However, the line shows a very high avarage σ width of 1.80±0.13 Å.

The broad line can be centroided to a wavelength accuracy of almost 1% and we find wavelengths which appear more consistent in obsids 10760, 10759, and 10857 at an average value of 17.7 Å (0.700 keV), but significantly different in obsid 10858 at 18.2 Å (0.681 keV). This indicates that the feature centroid is variable. Furthermode, we cannot identify a single responsible ion at these wavelengths. If it is a wavelength complex it has to include major lines we expect in this region, which are expected to be predominantly from Fe XVII and the O VII and O XVIII Lyman series. However, we simulated several cases of broad line complexes using the embedded XSTAR function *photemis*, which is available in the most recent *Xspec* version as a local module, and find that Fe XVII cannot contribute because we do not observe a significant contribution of the most prominent line at 15 Å. The most likely solution is the O XVIII Lyman series with a dominant contribution from the O XVIII Lyman α line. The rest wavelength of this line is 18.97 Å (0.656 eV) and the measured centroid position then appears significant blue-shifted between 0.77 Å and 1.27 Å.

An identification with a single O VIII L$_\alpha$ line leads to velocity broadening of almost 3.0×10^4 km s^{-1}, which has to be considered relativistic. As done for the *XMM-Newton* RGS data (Madej et al. 2010) we fit this line feature with a gravitationally broadened line model *laor* (Laor 1991) available in *Xspec*. The fits are summarized in Table 3. The model contributes to the fits at least as well as the broad gaussian with some improvement in the soft residuals. For 1540 d.o.f. we obtain reduced χ^2_{nu} between 1.37 and 1.63 in the band

between 1.7 and 25Å. The *laor* fits produce two fit solutions with respect to inclination which appear equivalent. In obsids 10857 and 10759 the fit finds a value around 86° and r_{in} of ~9, in obsids 10760 and 10858 values of 89° and r_{in} of ~2 are preferred. In Table 3 we fixed the inclination to 86°. The fits also show line wavelengths blue-shifted with respect to the O VIII L_α line rest wavelength by amounts similar to the one observed in the gaussian fits of up to 6%. While the *laor* model predicts a blue-shift due to gravitiational effects, shifts in Table 3 still appear significantly variable up to 70%.

4.   Discussion

Our analysis shows that 0614 is observed in a hard state. The continuum is dominated by a powerlaw of index of about 2.2 similar to the one suggested by Piraino et al. (1999) and very recently by Madej et al. (2010). We also confirm the need for a hard blackbody of about 1.2 keV as suggested by Piraino et al. (1999) and Migliari et al. (2010). However, the spectra do not show a dominant disk blackbody component as found by Migliari et al. (2010) in *SWIFT* data. On the other hand, we searched for an Fe K edge as suggested by Piraino et al. (1999) indicating the existence of a highly absorbed high energy component to no avail.

0614 has been classified as an ultra-compact binary system. Specifically the detection of an excessive Ne K edge in an early *Chandra* observation (Paerels et al. 2001) sparked interpretations that in combination with a possible ultra-short orbital period the donor stars are C-O or O-Ne-Mg stars (Juett, Psaltis & Chakrabarty 2001). Our observations indeed confirm the existence excess Ne K edge optical depth. A recent VLA study on the other hand finds a rather different account and observed Ne II and III emissions which suggested Ne to be underabundant (Werner et al. 2006). Our new observations show that the Ne K edge clearly shows an excess source intrinsic component. The edge is highly variable which is evidence that the excess Ne is source intrinsic. We conclude on this basis that 0614 indeed shows a Ne excess abundance. Whether this overabundance is restricted to Ne alone is uncertain. In at least one observation we find excess Mg as well. For other elements we do not find any conclusive overabundance signatures.

Another aspect of our study is the dynamic appeearence of the edge. We find a smeared edge which we approximate by blue- and redhsifted components. To our knowledge this is the first time this kind of dynamics has been observed in a cool K edge. We tested this dynamics with known periodicities (Shahbaz et al. 2008) and conclude that it is random in nature. The Ne edge shows systematic blue- and red-shifts at average Doppler velocities of around 3500 km s^{-1}. If we associate this cool absorbing material with an extended outer

edge rim of the accretion disk and near edge-on view we can infer an upper limit to the outer radius of the disk of less than 10^9 cm (or <3500 km s^{-1}) consistent with an ultra-compact binary. In order to make this feasibkle we have to assume that the disk radius is small enough in order to have X-ray with blue- and red-shifted absorption scattered in our line of sight. This may not be unfeasible but needs future detailed modeling. The random appearance of optical depth variations as well as edge shifts may also signal the presence of heavy turbulence of cool plasma entering the accretion resulting in heavy convulsions producing red- and and blue-shifts at times.

There is at least one broad line emission line complex in the spectra near ionized oxygen, which has already been seen in several previous observations with *EXOSAT* (Singh & Apparao 1994), *ROSAT* (Schulz 1999), *BeppoSAX* (Piraino et al. 1999), and *SWIFT* (Migliari et al. 2010). In neither of these obervations could the line be resolved because of insufficient instrument resolution. Even though the HETG in our study fully resolves the line, it still finds it broad on previously suggested levels and does not show structure. We find the width between 50 and 66 eV similar to previous studies. Very recent *XMM-Newton* observations also find a single broad line in RGS spectra (Madej et al. 2010) and it is quite obvious that the line feature cannot be further resolved.

The line location suggests that it is dominated by O VIII L$_\alpha$ with maybe some contribution of O VII L$_\beta$ and O VIII L$_\beta$ emission. A single gaussian line interpretation leads to Doppler velocities of the order of 3×10^4 km s^{-1}, which is 10% of the speed of light and here we need to include relativistic effects such as gravitational (GR) broadening. Madej et al. (2010) successfully fit a GR profile to the line providing a line centroid of 18.5Å, an inner radius of 3.5 R$_g$, and a line of sight inclination of 88°. Our fits to the four observation segments give similar results, however also produce a larger spread of values. The inclination angles appears to be similar, an averaged value gives 87.5°.

If these broad lines originate from the accretion disk, a viewing angle near 90° makes sense and is already argued for in Migliari et al. (2010). In general, disk velocities of 3×10^4 km s^{-1} already require disk radii of a few 10^7 cm and significantly lower inclination values would push the emission site beyond the inner edge of the disk. With a source luminosity of 0.02 L$_{edd}$ this requires ionization parameters far beyond 10^4 and consequently barely allow for ionization fractions for H-like ions. We have observed high ionization parameters in the high flux state of Cir X-1, where edge-on viewing also seems likely (Brandt & Schulz 2000; Schulz et al. 2008). However, there the higher luminosities produce measurable ionization fractions at much larger disk radii. In the case of 0614 lower inclinations thus would lead to unrealistic dynamics, emission radii, and ionization parameters. We see some resemblance to the case of 4U 1626-67 (Schulz et al. 2001; Krauss et al. 2007), which being viewed face

on already revealed disk (v sin i) velocities of several thousand km s^{-1}. 4U 1626-67 viewed edge-on would also likely show high velosity broadening in its lines. Recently the presence of soft broad line emission has also been reported in the Z-sources GX 349+2 (Iaria et al. 2009) and Cyg X-2 (Schulz et al. 2009).

An identification of O VIII L$_\alpha$would also imply blue-shifts larger than 0.5 Å independent of the line model. Even though the gravitational model predicts some blue-shift (Laor 1991), it should be consistent in all observations. However, the observed line wavelengths show significant variations indicating some additional dynamics in the line emitting region. Furthermore, *Chandra* lines show consistently higher blus-shifts compared to the *XMM-Newton* measurement (Madej et al. 2010). Possibilities may include changes in ionization balance, variable Compton scattering, or inner disk outflows. Changes in ionization balance are not obvious as observed spectral and flux changes do not appear dramatic. Compton upscattering requires very high optical depths as can be found in the disk but should lead to some tail on the blue side of the line which is not obvious in our data. An outflow interpretation remains viable, but needs more detailed modeling in order to quantify further. The difference in shift is about 0.7 Å corresponding to an order of 10^4 km s^{-1}. Observed outflow velocities of this amount are rare in Galactic binaries, though. Winds and outflows in X-ray binaries are now commonly observed, mostly in systems exhibiting strong X-ray luminosities, such as in Cir X-1 (Brandt & Schulz 2000; Schulz & Brandt 2002), GX 13+1 (Ueda et al. 2004) or the blackhole binary GRS J1655-40 (Miller et al. 2006), but all at much lower velocities. However, strong outflows of several 1000 km s^{-1} now also have been observed in sub-Eddington accretors such as 4U 1822-37 (Bayless et al. 2010) and Her X-1 (Boroson et al. 2007) in UV spectra. 0614 has gained a reputation in recent years of being of specifically violent nature showing sporadic abnormal type I superbursts (Kuulkers, in't Zand & Lasota 2009) and an active jet during its hard state quite similar to what is commonly observed in black hole binaries (Migliari et al. 2010).

There are also several issues with respect to the observed abundances in the spectra. If 0614 is indeed ultra-compact we would expect that the donor star is either a C-O or O-Ne or similar white dwarf. In this respect it makes sense that we observe prodominantly neon and oxygen-rich matter in the accretion disk. However, some of the findings raise more questions. First of all, if we indeed see highly ionized oxygen in the inner disk, why are there no similar Ne IX and Ne X emissions. The emissivity distributions with respect to temperature of these ions strongly overlap and, like in the case of 4U 1626-67 , we whould observe similar strong emissions from O and Ne. Our spectra allow for broad line flux upper limits at Ne IX and Ne X wavelengths which are over an order of magnitude fainter than what we observe in O VIII L$_\alpha$ which does not provide an answer to the problem. Likewise, our analysis of the K edges reveals significant excesses in the Ne K columns, but not in the O K columns. At

radii of the order of 10^9 cm and the observed source luminosities we do not expect ionization parameters high enough to destroy all neutral oxygen.

Even though we lack answers to many of our findings, we tentatively conclude the following:

- 0614 shows a variable excess Ne absorption column densities of up to several 10^{18} cm^{-2}

- The overabundance has a dynamic high velocity component and is evidently source intrinsic

- The Ne K edge velocity smear could point to a probable outer disk radius limit of several 10^9 cm supporting an ultra-compact binary nature

- The soft X-ray line emission appears extremely broad with corresponding velocities of 3×10^4 km s^{-1} and likely originates from a relativistic disk regime.

- The line emission indicates an ionized disk layer, predominantly O VIII L$_\alpha$, at radii well below 10^8 cm down to only several gravitational radii.

- The soft X-ray line emission shows variable blue-shifts with respect to the O VIII L$_\alpha$ rest wavelength indicating further dynamical processes near the inner disk.

REFERENCES

Bayless, A. J., Robinson, E. L., Hynes, R. I., Ashcraft, T. A., & Cornell, M. E., 2010, ApJ, 709, 251

Boroson, B. S., Vrtilek, S. D., Raymond, J. C., & Still, M., 2007, ApJ, 667, 1087

Brandt, S., Castro-Tirado, A. J., Lund, N., Dremin, V., Lapshov, I., & Syunyaev, R., 1992, A&A, 262, L15+

Brandt, W. N., & Schulz, N. S., 2000, ApJ, 544, L123

Fiocchi, M., Bazzano, A., Ubertini, P., Bird, A. J., Natalucci, L., & Sguera, V., 2008, A&A, 492, 557

Ford, E. C., et al., 1997, ApJ, 486, L47+

Forman, W., Jones, C., Cominsky, L., Julien, P., Murray, S., Peters, G., Tananbaum, H., & Giacconi, R., 1978, ApJS, 38, 357

Gorczyca, T. W., 2000, Phys. Rev. A, 61, 024702

Iaria, R., D'Aí, A., di Salvo, T., Robba, N. R., Riggio, A., Papitto, A., & Burderi, L., 2009, A&A, 505, 1143

Juett, A. M., & Chakrabarty, D., 2005, ApJ, 627, 926

Juett, A. M., Psaltis, D., & Chakrabarty, D., 2001, ApJ, 560, L59

Juett, A. M., Schulz, N. S., & Chakrabarty, D., 2004, ApJ, 612, 308

Juett, A. M., Schulz, N. S., Chakrabarty, D., & Gorczyca, T. W., 2006, ApJ, 648, 1066

Krauss, M. I., Schulz, N. S., Chakrabarty, D., Juett, A. M., & Cottam, J., 2007, ApJ, 660, 605

Kuulkers, E., in't Zand, J. J. M., & Lasota, J., 2009, A&A, 503, 889

Laor, A., 1991, ApJ, 376, 90

Linares, M., van der Klis, M., & Wijnands, R., 2008, in AAS/High Energy Astrophysics Division, Vol. 10, 10.17

Madej, O., Jonker, P., Fabian, A., Pinto, C., Verbunt, F. W. M., & de Plaa, J., 2010, http://www.sron.nl/index.php?option=com_content&task=view&id=2665&Itemid=2354, 0

Mendez, M., van der Klis, M., van Paradijs, J., Lewin, W. H. G., Lamb, F. K., Vaughan, B. A., Kuulkers, E., & Psaltis, D., 1997, ApJ, 485, L37+

Migliari, S., et al., 2010, ApJ, 710, 117

Miller, J. M., Raymond, J., Fabian, A., Steeghs, D., Homan, J., Reynolds, C., van der Klis, M., & Wijnands, R., 2006, Nature, 441, 953

Paerels, F., et al., 2001, ApJ, 546, 338

Piraino, S., Santangelo, A., Ford, E. C., & Kaaret, P., 1999, A&A, 349, L77

Schulz, N. S., 1999, ApJ, 511, 304

Schulz, N. S., & Brandt, W. N., 2002, ApJ

Schulz, N. S., Canizares, C. R., Lee, J. C., & Sako, M., 2002, ApJ, 564, L21

Schulz, N. S., Chakrabarty, D., Marshall, H. L., Canizares, C. R., Lee, J. C., & Houck, J., 2001, ApJ, 563, 941

Schulz, N. S., Huenemoerder, D. P., Ji, L., Nowak, M., Yao, Y., & Canizares, C. R., 2009, ApJ, 692, L80

Schulz, N. S., Kallman, T. E., Galloway, D. K., & Brandt, W. N., 2008, ApJ, 672, 1091

Shahbaz, T., Watson, C. A., Zurita, C., Villaver, E., & Hernandez-Peralta, H., 2008, PASP, 120, 848

Singh, K. P., & Apparao, K. M. V., 1994, ApJ, 431, 826

Swank, J. H., Boldt, E. A., Holt, S. S., Serlemitsos, P. J., & Becker, R. H., 1978, MNRAS, 182, 349

Ueda, Y., Murakami, H., Yamaoka, K., Dotani, T., & Ebisawa, K., 2004, ApJ, 609, 325

van Straaten, S., Ford, E. C., van der Klis, M., Méndez, M., & Kaaret, P., 2000, ApJ, 540, 1049

Verbunt, F., & van den Heuvel, E. P. J., 1995, in X-ray binaries, p. 457 - 494, ed. W. H. G. Lewin, J. van Paradijs, & E. P. J. van den Heuvel, 457

Werner, K., Nagel, T., Rauch, T., Hammer, N. J., & Dreizler, S., 2006, A&A, 450, 725

Wilms, J., Allen, A., & McCray, R., 2000, ApJ, 542, 914

TABLE 1: CHANDRA HETGS X-RAY OBSERVATIONS IN 2009

Obsid	Start Date [UT]	Start Time [UT]	Exposure [ks]	HETG 1st rate cts s^{-1}
10760	Jan 18 2009	23:07:34	44.1	13.89
10858	Jan 19 2009	17:45:01	34.4	12.33
10857	Jan 21 2009	13:49:21	57.3	9.90
10759	Jan 24 2009	05:07:34	60.3	24.29

TABLE 2 SPECTRAL FIT: POWERLAW + BBODY + GAUSSIAN LINE PARAMETERS

OBSID	A_{pl}	Γ	A_{bb}	kT_{bb}	A_{line}	λ_{line}	σ_{line}
	ph Å^{-1} cm^{-2} s^{-1}	–	10^{36} erg s^{-1}/D^2_{10kpc}	keV	ph cm^{-2} s^{-1}	Å	Å
10760	$0.450^{0.006}_{0.006}$	$2.244^{0.009}_{0.009}$	$0.76^{0.06}_{0.05}$	$1.360^{0.114}_{0.153}$	$0.062^{0.005}_{0.003}$	$17.752^{0.176}_{0.177}$	$1.748^{0.132}_{0.137}$
10858	$0.368^{0.007}_{0.003}$	$2.211^{0.013}_{0.008}$	$1.04^{0.05}_{0.05}$	$1.294^{0.091}_{0.026}$	$0.065^{0.002}_{0.001}$	$18.193^{0.144}_{0.155}$	$2.066^{0.167}_{0.133}$
10857	$0.599^{0.006}_{0.005}$	$2.134^{0.006}_{0.008}$	$1.04^{0.05}_{0.05}$	$1.389^{0.091}_{0.096}$	$0.056^{0.009}_{0.006}$	$17.534^{0.118}_{0.134}$	$1.729^{0.111}_{0.139}$
10759	$0.415^{0.005}_{0.004}$	$2.246^{0.008}_{0.007}$	$1.04^{0.05}_{0.05}$	$1.389^{0.091}_{0.096}$	$0.058^{0.005}_{0.004}$	$17.835^{0.165}_{0.147}$	$1.755^{0.117}_{117}$

TABLE 3 SPECTRAL FIT PARAMETERS OF A RELATIVISTIC LAOR PROFILE

OBSID	A_l ph Å^{-1} cm^{-2} s^{-1}	E_l keV	λ_l Å	r_{in} GM/c^2	Incl. deg.	χ^2_{nu}
10760	$0.063^{0.004}_{0.003}$	$0.685^{0.001}_{0.004}$	$18.10^{0.10}_{0.03}$	$12.87^{0.36}_{2.05}$	86	1.62
10858	$0.064^{0.003}_{0.007}$	$0.672^{0.002}_{0.001}$	$18.44^{0.05}_{0.04}$	$10.85^{2.15}_{1.33}$	86	1.27
10857	$0.062^{0.003}_{0.004}$	$0.698^{0.001}_{0.001}$	$17.76^{0.04}_{0.02}$	$9.47^{1.64}_{0.59}$	86.2±0.5	1.37
10759	$0.057^{0.005}_{0.004}$	$0.694^{0.002}_{0.001}$	$17.88^{0.03}_{0.06}$	$8.02^{1.04}_{1.01}$	86.1±0.5	1.63
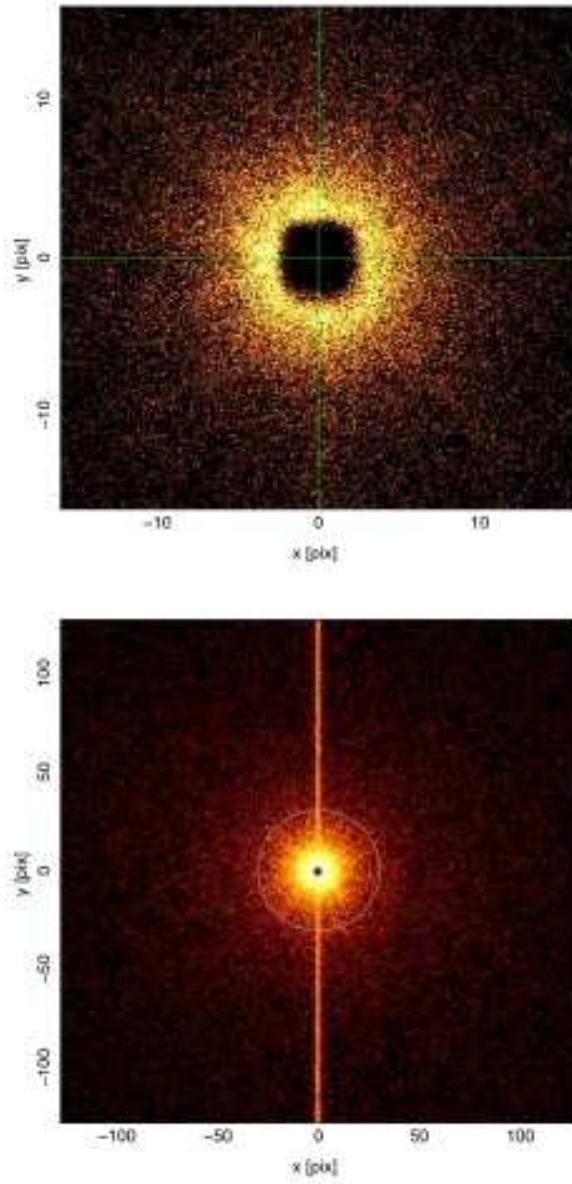
Fig. 1.— The zero oder image of OBSID 10759. The cross in the top image shows the exact zero order position. In the bottom its exact coincidence with the readout streak.
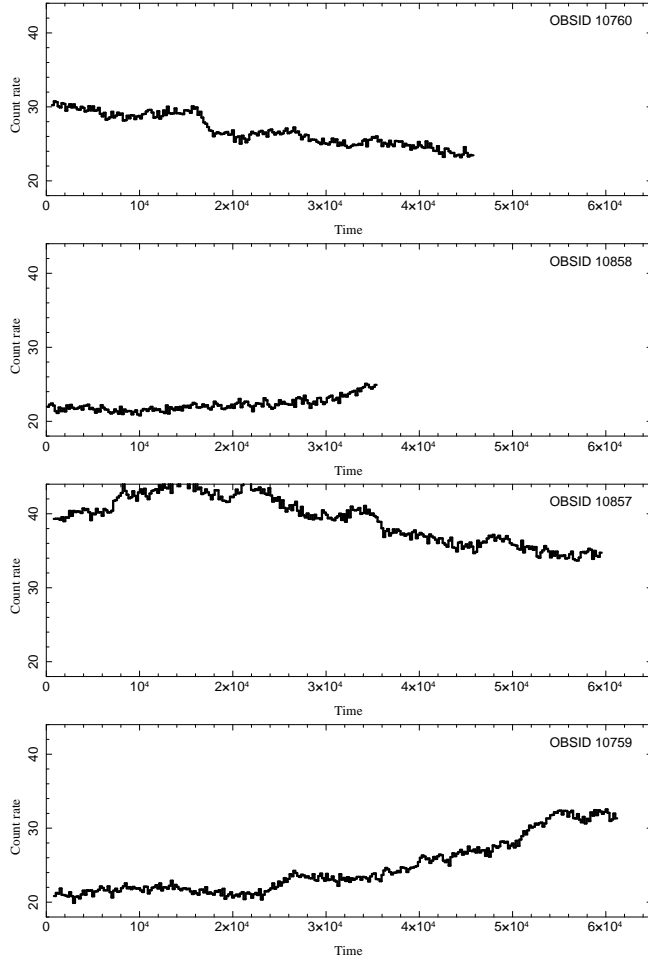
Fig. 2.— The light curves of the four observations. Data bins of 200 sec contain all HETG 1st order photons from 1.6 to 25 Å.
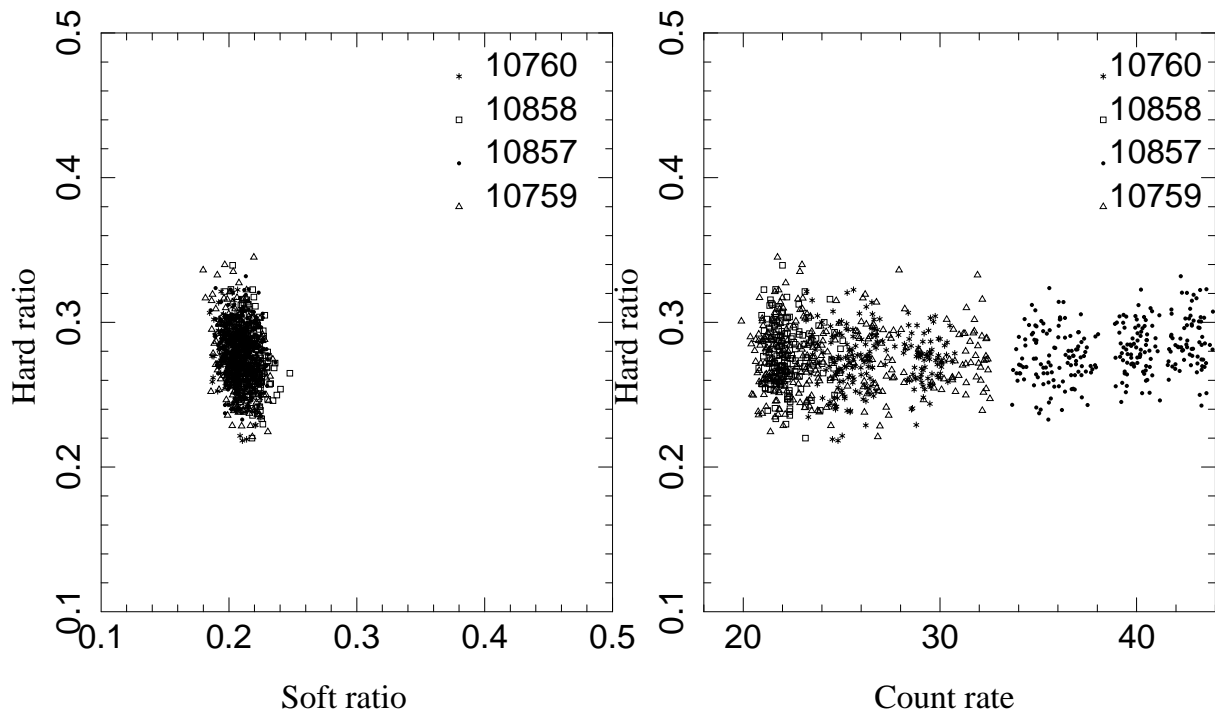
Fig. 3.— **Left:** The HETG 1st order color-color diagram for the four observations. Each data point represents 200 sec of integration time. Corresponding error bars amount to about ±0.02 on each scale. **Right** The corresponding hardness-intensity diagram.
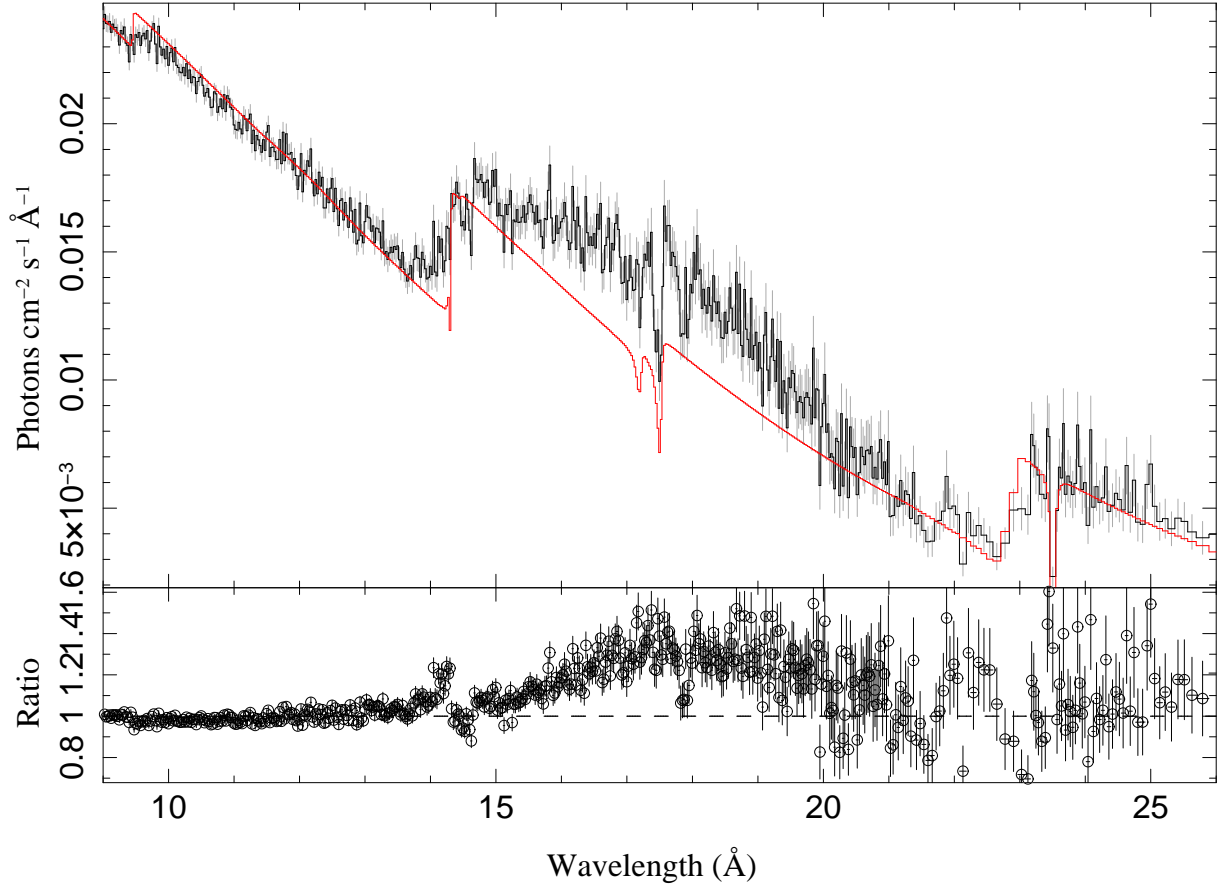
Fig. 4.— The soft X-ray spectrum of obsids 10759 and 10760. The continuum is a powerlaw (see Table 2) with an optical depth adjustment of the Ne K edge. For the ISM absorption we used the most recent *Tbnew* function in *XSPEC* which includes the substructure at the Ne and O K edges and the Fe L edge. The fit also includes a broad Gaussian line near 18Å. For illustration purpose we removed the line contribution from the model and residals. The Ne K also leaves a residual since we do not include any wavelength adjustments.
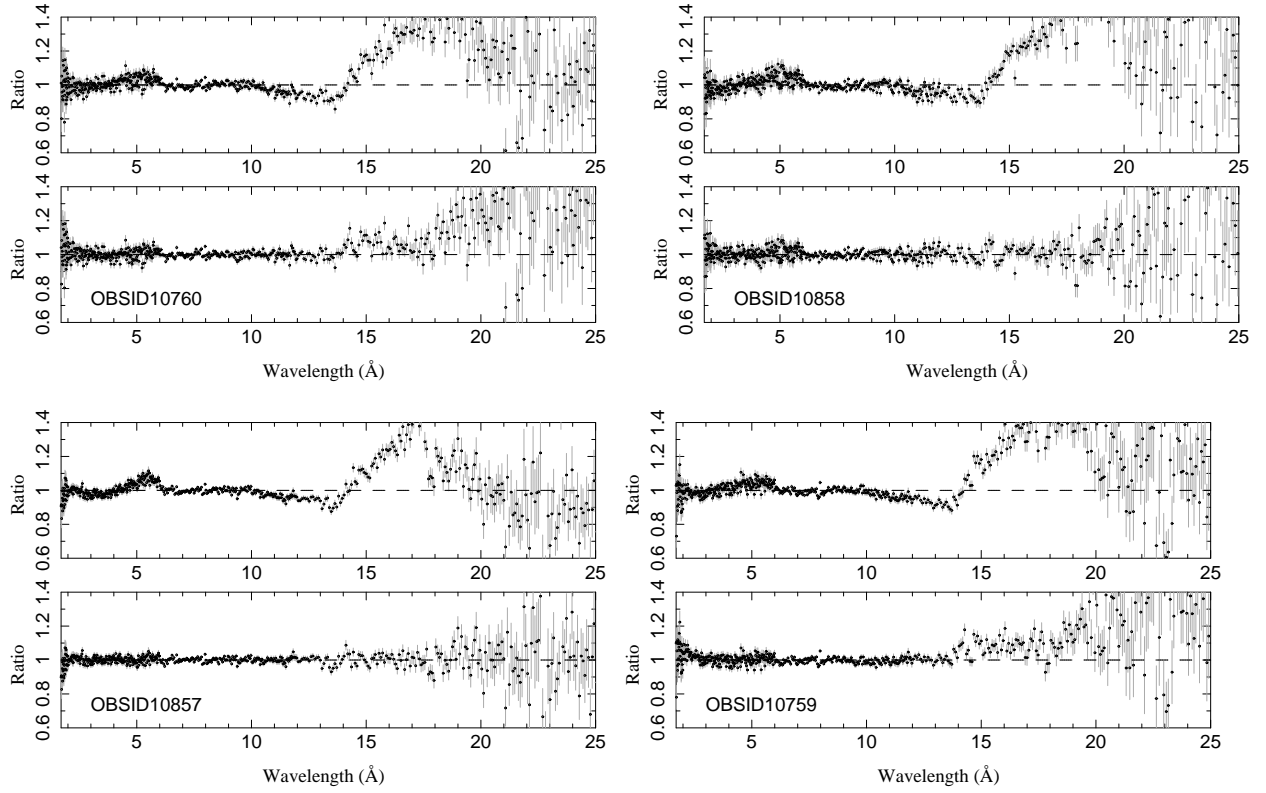
Fig. 5.— Residuals from continuum fits with and without additional K edge depths and broad line emission. A large impact on the fits comes from an adjustment of the Ne K edge (14.29 Å) depth and the addition of a very broad Gaussian line function around 18 Å. Some minor impact arises from an adjustment of the Mg K depth and another much weaker broad line between 11 and 12 Å.
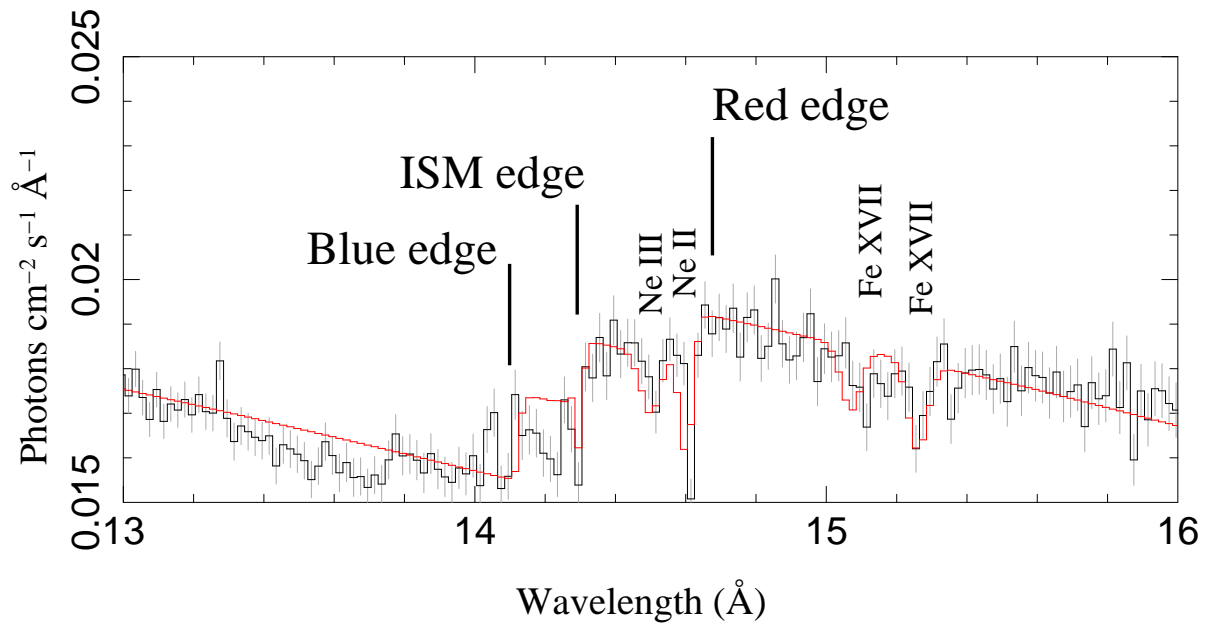
Fig. 6.— Local Ne K edge of the total exposure summed over the four observations. The edge is very complex showing red- and blue- shifted components in addition to the ISM contribution. The red- and blue-shifted components are smeared as the edge is changing at timescales smaller then 1000 sec. The red portion of the edge is also perturbed by existing Ne IIand Ne IIIlines.
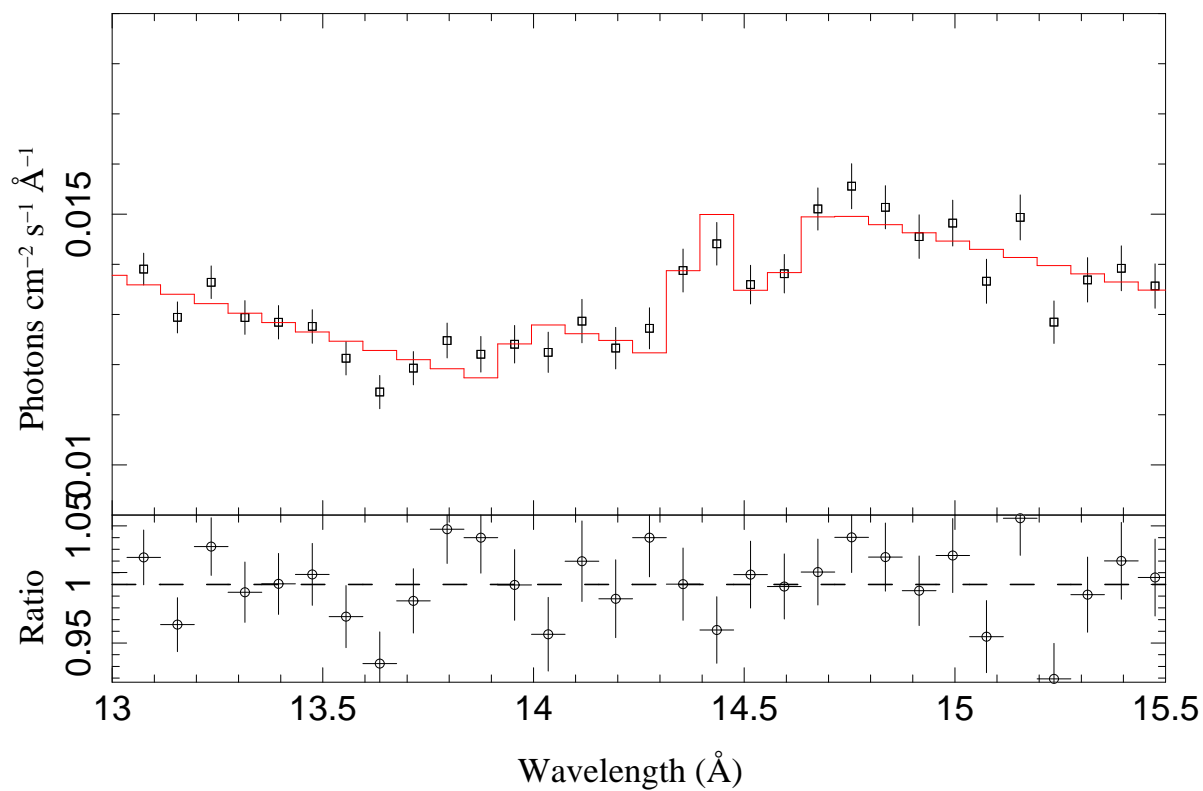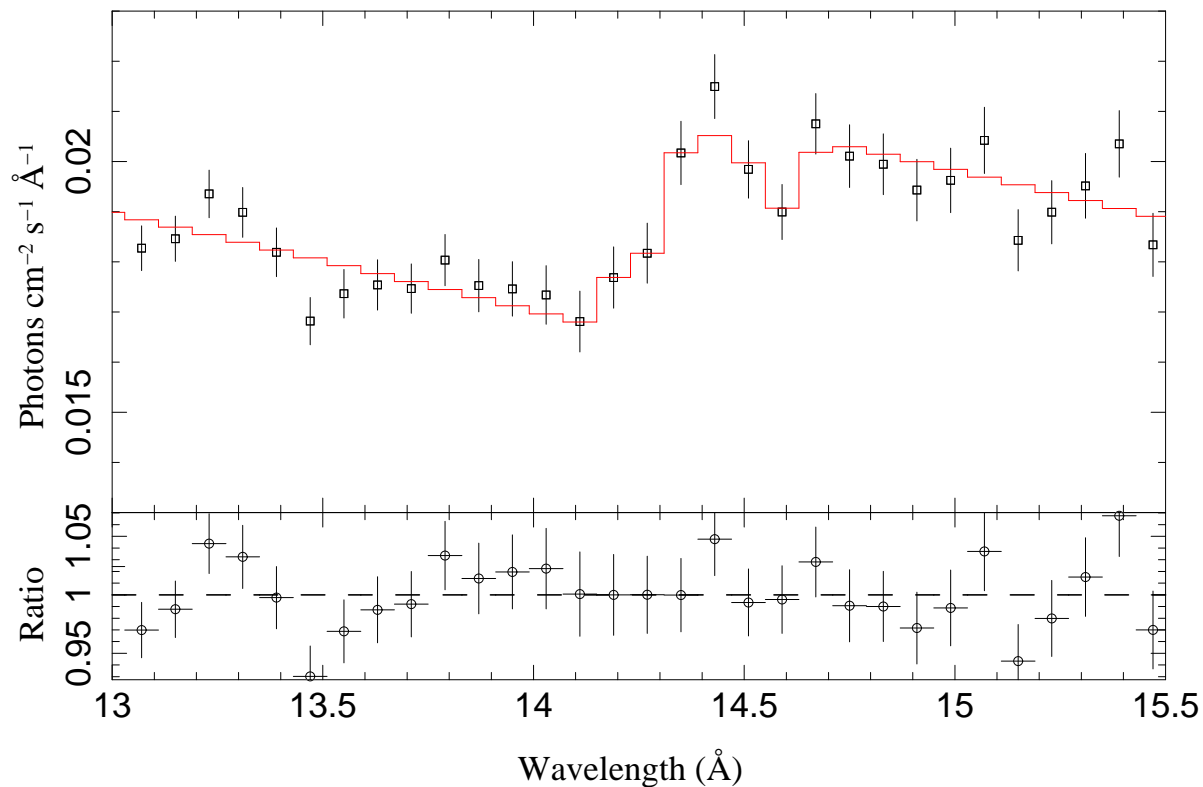
Fig. 7.— Two cases of edge morphology for a very low (top) and very large (bottom) velocity smear of the Ne K edge. Here we integrated three extreme sub-segments in each case. Average excess total optical depths vary from 0.10 to 0.14, blue- and red-shifts from 0.08 to 0.24 mA.
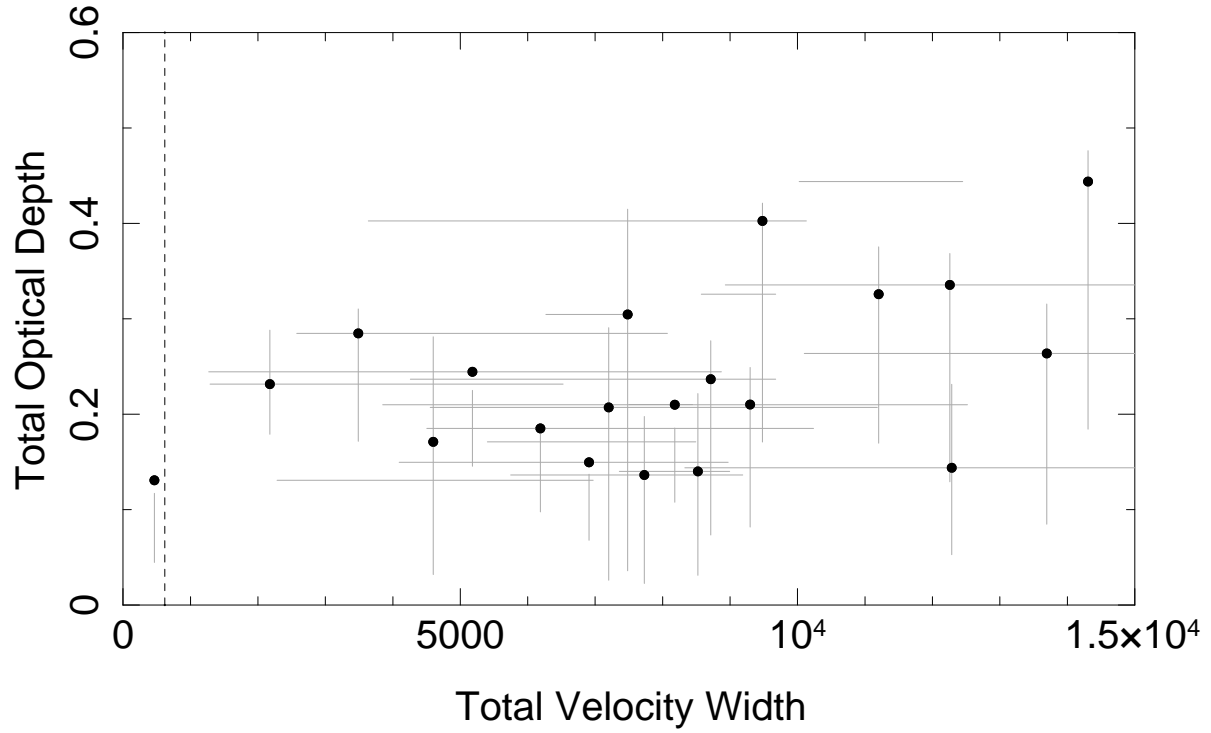
Fig. 8.— The total velocity spread (blue- and red-shifts) plotted against the total intrinsic edge optical depth. The dotted line marks the likely amount of a velocity smear from an orbital period of 51.3 min Shahbaz et al. (2008).